Molecular Visualization of the Yeast Dmc1 Protein Ring and Dmc1−ssDNA Nucleoprotein Complex†

Yuan-Chih Chang,‡ Yu-Hui Lo,§ Ming-Hui Lee,§ Chih-Hsiang Leng,§ Su-Ming Hu,§ Chia-Seng Chang,*,‡ and Ting-Fang Wang*,§

Institute of Biological Chemistry and Institute of Physics, Academia Sinica, Taipei 11529, Taiwan

Received May 28, 2004; Revised Manuscript Received January 27, 2005

ABSTRACT: *Saccharomyces cerevisiae* Dmc1, a meiosis-specific homologue of RecA, catalyzes homologous pairing and strand exchange during meiotic DNA recombination. The purified budding yeast Dmc1 (ScDmc1) protein exhibits much weaker recombinase activity in vitro as compared to that of the *Escherichia coli* RecA protein. Using atomic force microscopy (AFM) with carbon nanotube tips, we found ScDmc1 forms rings with an external diameter of 18 nm and a central cavity of 4 nm. In the presence of single-stranded DNA (ssDNA), the majority of the ScDmc1 protein (90%) bound DNA as protein rings; only a small faction (10%) was able to form filamentous structure. In contrast, nearly all RecA proteins form fine helical nucleoprotein filaments with ssDNA under identical conditions. RecA-mediated recombinase activity is initiated through the nucleation of RecA onto ssDNA to form helical nucleoprotein filaments. Our results support the notion that ScDmc1 becomes catalytically active only when it forms a helical nucleoprotein filament with ssDNA.

In *Saccharomyces cerevisiae*, meiotic DNA recombination is initiated by DNA double-strand breaks (DSBs)[1] (*1*, *2*). DSBs with 5′ termini are processed to produce 3′-overhanging single-stranded DNA (ssDNA) tails. These processed DNA ends are then resolved via strand assimilation and exchange into two types of recombination products: reciprocal crossovers and noncrossovers. Two long-lived post-DSB intermediates have been described: one in which a single end forms a stable joint with the homologue (i.e., single-end invasion) and a second in which both ends are incorporated into the homologue to form a fully ligated double-Holliday junction. Recent studies suggest that both single-end invasion and double-Holliday junction are crossover intermediates (*3*−*5*), and post-DSB noncrossover intermediates are yet to be detected.

Homologous pairing and strand exchange reactions are thought to be catalyzed by two RecA-like recombinases, Rad51 and Dmc1 (*6*). In *S. cerevisiae*, the expression of Dmc1 is limited to meiosis, whereas Rad51 is expressed in both mitosis and meiosis. Both proteins are required for DNA recombination during meiosis in vivo (*7*, *8*). Biochemical analysis indicates that these two proteins exhibit higher binding affinity for ssDNA than for dsDNA and are able to catalyze assimilation of ssDNA into dsDNA (*8*−*12*).

Rad51, like *Escherichia coli* RecA, forms helical nucleoprotein filaments with DNA substrates. The pitch of DNA in RecA helical filaments is stretched and untwisted from ∼36 Å (in B-form) to ∼95 Å (*13*−*15*). In the absence of DNA, both RecA (*14*, *16*) and Rad51 (*17*) form hexameric rings that appear to be structural homologues of the hexameric DNA helicase. Since neither function nor DNA binding has yet been demonstrated for the ring form of RecA and Rad51, it was assumed that only the active RecA and Rad51 proteins form helical nucleoprotein filaments and subsequently initiate homologous pairing and strand exchange reactions. The crystal structure of a *S. cerevisiae* Rad51 filament formed by a gain-of-function mutant was recently determined, providing more clues about the mechanism of allosteric communication between ATPase- and DNA-binding sites (*18*). This filament exhibits a breakdown of 6-fold symmetry such that alternating ATPase sites are in slightly different environments, suggesting that this filament can exhibit at least two different apparent affinities for nucleotides. Finally, the pitch (∼130 Å) of this Rad51 mutant protein filament is longer than that seen in the RecA protein (∼83 Å) (*19*). Given the somewhat wide range of filaments revealed by previous electron microscopy (EM) studies (*13*), the Rad51 filament is clearly very flexible. This structure feature likely represents a conformation that is accessible to related homologous recombinases during the catalysis of strand exchange (*18*). This supposition is supported by RadA, an archaeal RecA-like protein, which can bind DNA in the absence of a nucleotide cofactor as an octameric ring and in the presence of ATP as a helical filament (*20*, *21*). Neutron scattering, atomic force microscopy (AFM), and EM studies suggested that the RadA−ssDNA−ATP filament has a pitch ∼90−100 Å with approximately six recombinase subunits (*20*, *21*). Like the Rad51 gain-of-function mutant, the RadA

† This work was supported by the National Science Council (Grant 93-2311-B-001-055 to T.-F.W.) and Academia Sinica (Grant AS92IBC3 to Andrew H.-J. Wang).

* To whom correspondence should be addressed. T.-F.W.: e-mail, tfwang@gate.sinica.edu.tw. C.-S.C.: e-mail, jasonc@sinica.edu.tw.

‡ Institute of Physics.

§ Institute of Biological Chemistry.

[1] Abbreviations: DSB, double-strand break; AFM, atomic force microscopy; ScDmc1, yeast Dmc1; HsDmc1, human Dmc1; dsDNA, double-stranded DNA; ssDNA, single-stranded DNA; AMP-PNP, adenosine 5′-(β,γ-imino)triphosphate; CNT, carbon nanotube; FWHP, full width at half-peak.

10.1021/bi048897q CCC: $30.25
Published on Web 04/02/2005

protein forms helical filaments in crystals and in aqueous solution (*22*, *23*). The crystal structure of RadA in complex with the ATP analogue 5′-(β,γ-imino)triphosphate (AMP-PNP) is a filament with a 106 Å pitch and six protein subunits per turn (*22*). DNA-binding sites are located in the proximity of the filament axis, whereas the ATP analogue is buried between two RadA subunits. These structural features are similar to those of RecA and Rad51 active filaments (*18*, *19*).

Dmc1 is very distinct from RecA or Rad51. Purified human Dmc1 (HsDmc1) has been reported to form a nucleoprotein complex composed of stacked octameric rings on DNA. Although no helical nucleoprotein filament has been detected for HsDmc1 (*24*, *25*), it was suggested that the stacked rings formed by HsDmc1 on DNA are likely to be functional (*26*). The finding that Dmc1 forms only rings was very surprising. First, at the amino acid level, human Rad51 (HsRad51) and Dmc1 (HsDmc1) are 52% identical. One would expect that Dmc1 would have properties almost identical to those of Rad51 proteins. In addition, helical filaments were considered to the biologically active form of RecA, RadA, and Rad51. Recently, the octameric ring structure of HsDmc1 was determined, giving more clues about the stability and functionality of the toroidal structure (*27*). The Glu258 amino acid residue in HsDmc1 protein is thought to be important in stabilizing the ring with hydrogen bonds. This amino acid residue is well-conserved in all the Dmc1 homologues but not in Rad51 homologues. The mutant HsDmc1 (E285A) was not able to promote the DNA assimilation reaction in vitro, supporting the possibility that the octameric rings could be a functional form of HsDmc1. Given that the amino acid residues that are important for DNA binding are mostly localized at the inner ring region, these authors further inferred that DNA likely passes through a HsDmc1 ring (*27*). This model was immediately questioned by a more recent EM study demonstrating that HsDmc1 can form a helical filament on ssDNA (*28*). Although HsDmc1 used in the latter study was active in a strand exchange assay, a relatively high concentration of salt and a narrow pH range were required to reveal this activity. In addition, the HsDmc1−ssDNA helical filaments were much shorter than those assembled with HsRad51 (*28*). Hence, it seems obvious that HsDmc1 filaments are very hard to detect. Because HsDmc1 filamentous structure had escaped several other researchers (*24*−*27*), it is of interest, probably also very important, to determine if Dmc1 from other species can also form helical filaments.

In this study, we applied AFM with carbon nanotube (CNT) tips to visualize *S. cerevisiae* yeast Dmc1 (ScDmc1) in association with ssDNA. Like HsDmc1, ScDmc1 bound both ssDNA and dsDNA. However, ScDmc1 is in fact a very weak recombinase; the maximum level reached in the D-loop formation assay was 1% (*10*). Although it seems very likely that ScDmc1 and HsDmc1 would share identical structural properties, little is known about the structure of ScDmc1. We find the catalytically active ScDmc1 proteins, like HsDmc1, form rings in the absence of a DNA substrate. Most ScDmc1 binds ssDNA as protein rings, while a small faction (~10%) of ScDmc1 forms filamentous structure on DNA. This unique structural feature could explain why ScDmc1 by itself is a weak recombinase in vitro.

EXPERIMENTAL PROCEDURES

Protein. We cloned ScDmc1 cDNA via the sticky end PCR method (*29*), and introduced it into an *E. coli* pET28 vector (Novagen) that adds a 5′ six-histidine tag. The plasmid was transformed into the *E. coli* BL(DE3)/pLys strain (Novagen), which carries a null mutation in the *recA* gene. A recombinant His_6−Dmc1 protein was expressed and purified as described previously (*10*). *E. coli* RecA protein was purchased from New England Biolabs.

ATPase Assay. ϕX174 virion ssDNA (0.3 mM in nucleotides) was incubated first at 37 °C in buffer E [20 mM HEPES (pH 7.5), 1 mM magnesium acetate, 1 mM dithiothreitol, 100 μg/mL bovine serum albumin, 120 mM NaCl, and 2 mM [γ-^{32}P]ATP] for 10 min. ATP hydrolysis was initiated by addition of ScDmc1 (3.0 μM) or *E. coli* RecA (1.0 μM) at 37 °C. At set times, 0.3 μL aliquots were withdrawn and spotted on thin-layer chromatography plates (PEI-cellulose, Sigma), and then developed in 1.0 M formic acid and 0.5 M LiCl (*30*). A phosphoimager (Molecular Dynamics) was used to quantify the release of $^{32}PO_4^{3-}$ from [γ-^{32}P]ATP.

DNA Strand Assimilation Assay. The method in this study was modified slightly as described previously (*10*). Plasmids pUC18-kan and GW1 (*31*) used for DNA assimilation assays were purified without DNA denaturation by lysozyme/Triton lysis followed by centrifugation in a cesium chloride/ethidium bromide density gradient (*32*). Oligonucleotides were end-labeled with [γ-^{32}P]ATP by T4 polynucleotide kinase (New England Biolabs). ^{32}P-labeled DNA was purified from the unincorporated nucleotide using a G25 MicroSpin column (Amersham BioSciences). Concentrations of nucleic acids are given in moles of nucleotides for oligonucleotide and ssDNA or moles of base pair for duplex DNA. Oligonucleotides P1655 and PA1656 are homologous to pUC18-kan and GW1, respectively: P1655, 5′-GCGGTGTAAATACCGCACAGATGCGTAAGGAGAAAATACCGCATCAGGCC; P1556, 5′-CGATATAGGTGACAGACGATATGAGGCTATATCGCCGATAGAGGCGACAT.

^{32}P-labeled oligonucleotides, P1656 or P1655, or both (3 μM each) were incubated with ScDmc1 (1 μM) in the presence of 1 mM magnesium acetate, 2 mM AMP-PNP, or ATP. Assimilation reactions were initiated by addition of an equal volume of a solution with two supercoiled plasmids (pUC18-Kan and GW1; 20 μM each). The reaction mixtures were incubated at 37 °C for 15 min; the reactions were stopped, and the mixtures were deproteinated by the addition of 0.25% SDS and 0.25 mg/mL proteinase K for 2 min. DNA from the reaction mixtures was then resolved on a 0.8% agarose gel in Tris-aceteate-EDTA buffer [40 mM Tris, 1 mM Na_2-EDTA, and 20 mM acetic acid (pH 8.0)] for 6 h at 4 V/cm. Gels were semidried with Whatman filter paper, and directly analyzed by Phosphoimaging.

AFM. ϕX174 virion ssDNA was linearized by hybridization of two oligonucleotides (SG197 and SG198) to create two HaeIII sites. The reaction mixture was run on an agarose gel. The ssDNA (872 nucleotides in length) was excised and purified using the Qiagen PCR kit. The ϕX174 ssDNA and its nucleotide sequence were obtained from New England Biolabs. Oligonucleotides SG197 and SG198 hybridize to ϕX174 ssDNA sequences, residues 4931−4960 and 421−450, respectively: SG197, 5′-GCATCAACAGGCCACAAC-

CAACCAGAACGT; SG198, 5′-TGAGCTTAATAGAG-GCCAAAGCGGTCCGGA.

AFM samples were prepared by placing 2.0 μL of a sample solution on freshly cleaved mica. The sample solution contains 0.5 nM protein (either ScDmc1 or RecA), 2 mM AMP-PNP, and ssDNA substrate (0 or 6 nM in moles of nucleotides). After 2 min, excess protein was removed by washing the sample with 5 mL of double-distilled water, and the samples were then air-dried in a tissue culture laminar flow hood. AFM images using carbon nanotube probes were recorded as previously described (*33*). To provide a gentler and less destructive measurement, probe-sample contact time was minimized with a tapping mode AFM machine. The shape of CNT tips was determined with a JEM-2000V high-resolution transmission electron microscope (JEOL). To ensure a flat background before image analysis, the image is flattened and plane-fitted with the aid of the microscope's analysis software (Digital Instrument, version 4.42r4).

We first measured diameters at half-maximal height of the individual molecules. The full width at half-peak (FWHP) was used to avoid overestimation of protein width (*34*). After two additional dimensions (height and length) of individual AFM images had been obtained, the molecular volumes of ssDNA and the RecA−ssDNA complex were calculated by treating the molecule as a segment of a sphere, using eq 1 (*34*):

$$V_i = (l/6)(3w^2 + h^2) \quad (1)$$

where w is the FWHP, l is the length, and h is the height. This method was validated first by determining the volume of a RecA subunit (molecular weight, 37 842) in the RecA−ssDNA nucleoprotein filament. A previous EM study had shown that RecA−ssDNA helical filaments contain six RecA monomers and 18 nucleotides per turn (*14*). Accordingly, the total molecular weight per turn is ~235000. Since the pitch of the RecA−ssDNA filaments is 9.5 nm, the total volume in each turn was calculated to be 171.5 nm^3. The average volume of the single RecA protein from our AFM measurements was calculated to be ~ 28.6 nm^3. This number is very close to that obtained for a globular protein similar in size (38.00 kDa) by AFM with a Nanosenor Pointprobe (~24.8 nm^3; *35*).

RESULTS

Purification and Functional Characterization of the ScDmc1 Protein. A previous report indicated that NH_2 addition of the His_6 tag does not affect the in vivo function of the ScDmc1 protein (*10*). His_6−ScDmc1 was cloned into phage T7 expression vector pET28a. The ScDmc1 proteins were overexpressed in *E. coli* cells, and the high-salt cell lysates were subjected to purification on Co(II) affinity resins that selectively retained the His_6-tagged polypeptides. The eluates contained predominantly a protein when examined by SDS−PAGE (Figure 1A). Western blot analysis using an anti-His_6 polyclonal antibody had confirmed that the protein contains the His_6 tag (data not shown). The purified ScDmc1 protein is catalytically active as revealed by both the ssDNA-dependent ATPase assay (Figure 1B) and the D-loop formation assay (Figure 1C). In the presence of the ϕX174 virion ssDNA substrate, the ATP turnover rate (k_{cat}) for yDmc1 was determined to be 0.67 min^{-1}, which is similar

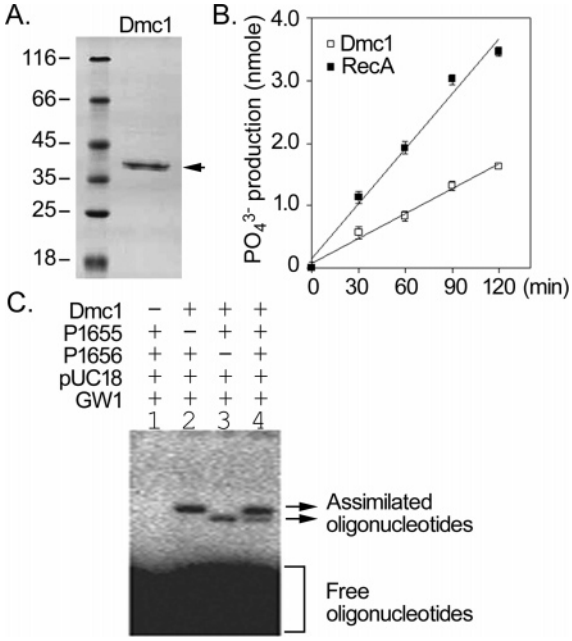

FIGURE 1: Purification and functional characterization of ScDmc1. (A) The purified His_6−ScDmc1 protein (500 ng) was analyzed by SDS−PAGE and visualized by Coomassie blue staining (indicated with an arrow). Positions of molecular size markers are shown in kilodaltons. (B) The ScDmc1 protein exhibits ssDNA-dependent ATPase activity. *E. coli* RecA [1.0 μM (■)] or ScDmc1 [3.0 μM (□)] was incubated with 0.2 mM [γ-^{32}P]ATP and 1 mM magnesium acetate in the presence of ϕX174 virion ssDNA (0.3 mM in nucleotides) at 37 °C. Aliquots (0.3 μL) were taken at the indicated time points, and then separated via thin-layer chromatography. ATP hydrolysis rates were determined by assessing the production of inorganic phosphate ($^{32}PO_4^{3-}$) using PEI chromatography and phosphorimaing. (C) The ScDmc1 protein catalyzes assimilation of ssDNA into supercoiled dsDNA plasmids in a homology-dependent manner. Oligonucleotides P1655 and P1656 were ^{32}P-labeled with T4 polynucleotide kinase. P1655 is homologous to plasmid pUC18-Kan; P1656 is homologous to plasmid GW1. ScDmc1 (1 μM) was preincubated with either P1656 (lane 2, 3 μM in nucleotides), P1655 (lane 3, 3 μM in nucleotides), or both (lane 4) before the addition of two dsDNA plasmids (20 μM in base pairs). No assimilated products were detected in the absence of ScDmc1 (lane 1). Reaction mixtures were deproteinated by addition of 0.25% SDS and 0.25 mg/mL proteinase K, respectively. The assimilated and free oligonucleotides were separated on a 0.8% agarose gel and developed as described in Experimental Procedures.

to the k_{cat} of hDmc1 (k_{cat} = 0.7 and 1.50 min^{-1}) (*21*, *22*) and yDmc1 (0.7 min^{-1}) (*10*) reported previously. The k_{cat} of *E. coli* RecA is 4.5 min^{-1}.

The ScDmc1 protein also promotes homology-dependent D-loop formation between P1656 and GW1 (Figure 1C, lanes 2 and 4) or between P1655 and pUC18-kan (Figure 1C, lanes 3 and 4), in a manner analogous to that described previously (*10*). Oligonucleotides P1655 and PA1656 (50 mers) are homologous to supercoiled plasmid DNA pUC18-kan and GW1, respectively. The formation of a DNA strand-assimilated product (or D-loop structure) in this reaction was detected by the presence of ^{32}P-labeled species with much lower electrophoretic mobility than the free ^{32}P-labeled oligonucleotides. Under the experimental conditions that were employed, maximal levels of D-loop formation were observed ~15 min after the supercoiled DNA and ScDmc1-coated ^{32}P-labeled oligonucleotides were mixed.

The results of both the ATPase assay and the D-loop formation assay support the notion that purified ScDmc1

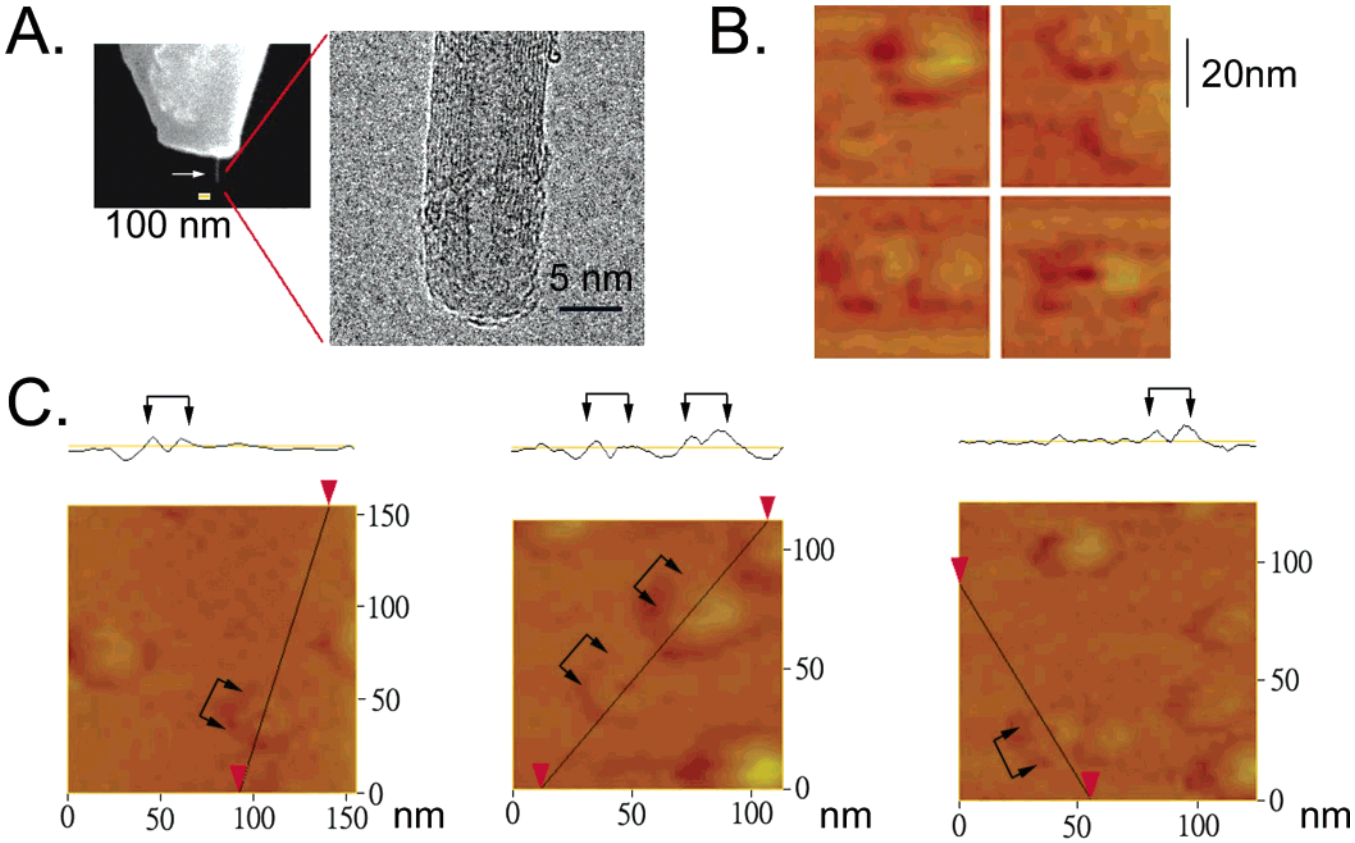

FIGURE 2: AFM−CNT visualization of the ScDmc1 proteins. (A) Scanning electron microscope images of a carbon nanotube (CNT) attached to a standard AFM tip (left panel). The white bar represents 100 nm. The white arrow denotes the CNT tip. The enlargement of the CNT tip image was from a high-resolution transmission electron microscope (right panel). The black bar represents 5 nm. (B) AFM topography of yDmc1 proteins observed with a CNT tip. (C) Height profiles of ScDmc1 protein rings. The vertical measurement of AFM topographies was carried out by cross-section analysis. Two arrows indicate the scanned region of a single ScDmc1 ring. The external diameter (18.0 ± 2.6 nm) and internal diameter (4.0 ± 1.2 nm) of yDmc1 rings were determined by FWHPs ($n = 50$).

proteins are catalytically active in vitro. These proteins are suitable for AFM structural analysis. Maximum strand assimilation activity was observed in the presence of AMP-PNP; only 10−20% of the maximum level of product formation was detected in the presence of ATP (data not shown and ref *10*). Therefore, AMP-PNP was used as the nucleotide cofactor in the following AFM image studies.

Ring Formation in the Yeast Dmc1 Protein. For the AFM study, ScDmc1 was diluted, spotted onto freshly cleaved mica, and then imaged using CNT tips. A high-resolution image of transmission EM indicates that the surface of the CNT tip used in this study is smooth with a tip radius of ∼5 nm (Figure 2A, right panel). These geometrical factors have been found to minimize tip−sample adhesion as well as tip−sample convolution, thereby maximizing the quality of the images (*36*).

We found that ScDmc1 proteins form aggregates in the absence of the DNA substrate, and ∼60% (50/82) of these protein aggregates can be clearly identified as rings (Figure 2B,C). Some ScDmc1 protein aggregates might not be recognized as rings, as a result of their orientation with respect to the surface; i.e., some are expected to stand on end with their central axis parallel. Cross-section analysis was carried out to estimate both lateral and vertical parameters. The FWHP was used here, because it represents a conventional definition of the width or diameter of AFM images. The external and internal diameters of the observed rings ($n = 50$) are 18.1 ± 2.6 and 4.0 ± 1.2 nm, respectively. The *Z* scale (or apparent height) of the ScDmc1 ring was 0.7 ± 0.1 nm (Figure 3C). The AFM volume of the ScDmc1 ring was estimated to be 170−220 nm^3. Because the molecular weight of His_6−ScDmc1 (37 819) is almost identical to that of RecA (37 842), the AFM volume of each ScDmc1 subunit should also be ∼25 nm^3 (see Experimental Procedures). Therefore, each ScDmc1 ring likely contains eight ScDmc1 subunits. Since HsDmc1 proteins also form octameric rings (*24*, *25*), it is likely that the structural organization of the Dmc1 protein is conserved from yeast to humans.

AFM Visualization of Yeast Dmc1−ssDNA Nucleoprotein Complexes. Having examined the shape of ScDmc1 alone, we then examined ScDmc1−ssDNA nucleoprotein complexes in the presence of AMP-PNP. The *E. coli* RecA protein was used here as a control for AFM experiments. AFM topography confirmed that RecA proteins indeed form fine helical filaments with ssDNA substrates (872 nucleotides in length). The pitch of RecA−ssDNA nucleoprotein filaments was determined to be 9−10 nm (Figure 3A). This result is consistent with previous EM data which show that the RecA−ssDNA filament has a pitch of 9.5 nm (*14*, *15*), indicating that experimental procedures in this study were not detrimental to protein samples and were of sufficient quality to resolve the fine helical structure of the RecA−ssDNA filaments.

The ScDmc1−ssDNA nucleoprotein complexes (Figure 3B,G) appeared to be more amorphous than the RecA−

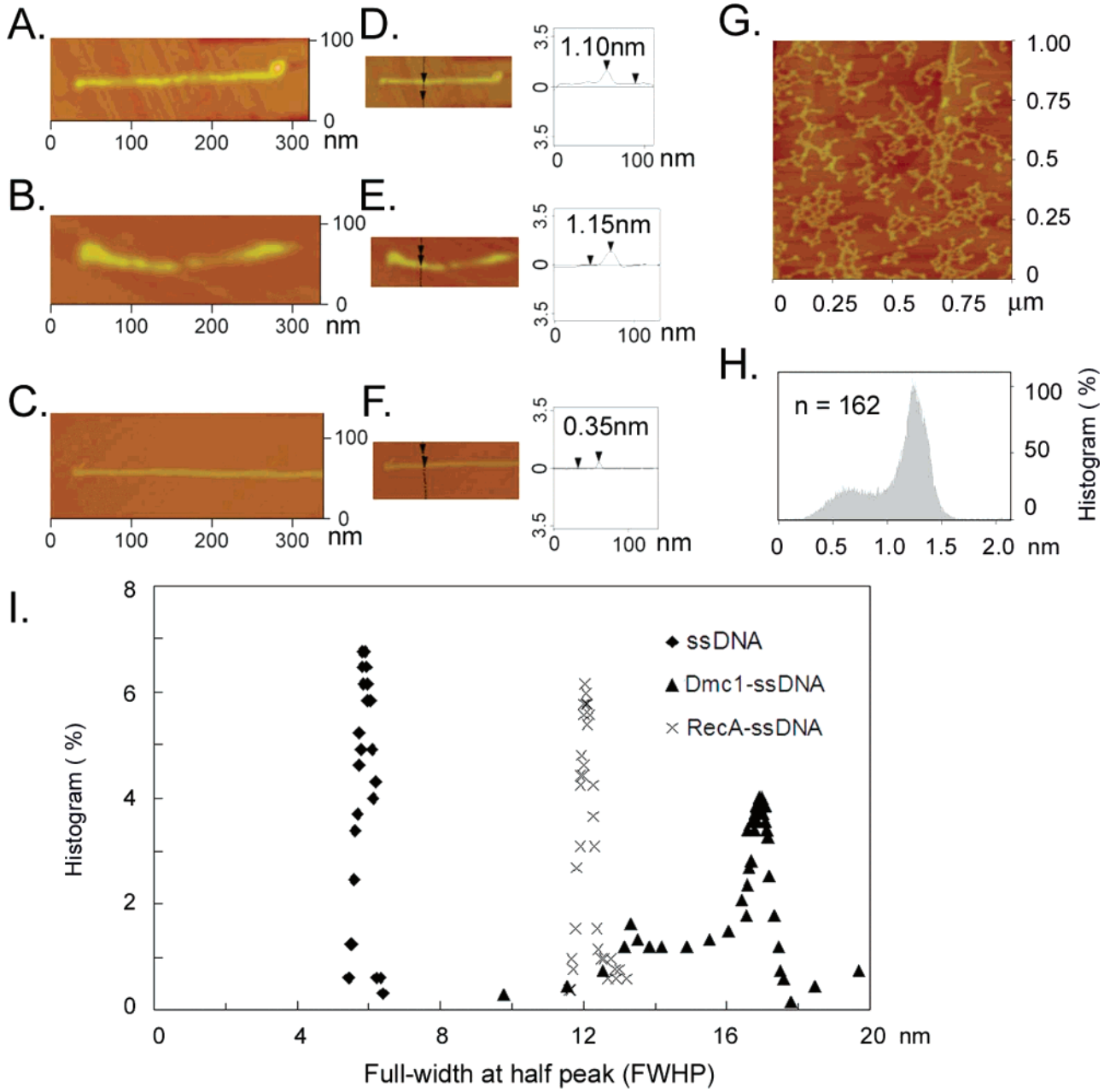

FIGURE 3: AFM−CNT visualization of ScDmc1−ssDNA nucleoprotein complexes. A ssDNA substrate (872 nucleotides in length) was incubated in the presence of 2 mM AMP-PNP with *E. coli* RecA (A) or ScDmc1 (B and G) or without an added protein (D) and then visualized by AFM using CNT tips (see Experimental Procedures). Height parameters were determined by cross-section analysis. Arrows indicate the scanned regions of RecA−ssDNA filaments (D), ScDmc1−ssDNA filaments (E), and naked ssDNA (F). Height parameters are given: 1.10 nm for RecA−ssDNA filaments, 1.12 nm for Dmc1−ssDNA filaments, and 0.35 nm for naked ssDNA. (H) Histogram analysis of height parameters of ScDmc1−ssDNA nucleoprotein complexes in panel G. The *X*-axis shows the height of the ScDmc1−ssDNA peak. The *Y*-axis shows the relative distribution frequency of 162 total height parameters. (I) Histogram analysis of FWHP values of different AFM images from RecA−ssDNA filaments, ScDmc1−ssDNA filaments, and ssDNA alone. The *X*-axis shows the FWHP. The *Y*-axis shows the relative distribution frequency of different FWHP values for ssDNA ($n = 325$), ScDmc1−ssDNA filaments ($n = 674$), and RecA−ssDNA filaments ($n = 510$). These FWHP values were obtained at different peaks by cross-section scanning analysis.

ssDNA filaments (Figure 3A) or naked ssDNA (Figure 3C). In contrast to RecA−ssDNA nucleoprotein filaments, no periodic structure can be clearly identified in ScDmc1−ssDNA filaments. Cross sections of AFM images revealed that the heights of RecA−ssDNA filaments (Figure 3D), ScDmc1−ssDNA filaments (Figure 3E), and naked ssDNA (Figure 3F) are 1.10, 1.15, and 0.35 nm, respectively. When more ScDmc1−ssDNA nucleoprotein complexes were visualized by AFM, almost all ScDmc1−ssDNA nucleoprotein complexes exhibit irregular structures (Figure 3G). Histogram analysis ($n = 162$ peaks) indicated that the heights of ScDmc1−ssDNA nucleoprotein filaments exhibit a bimodal distribution (Figure 3H). The first peak (~0.7 nm in height) represents the ScDmc1 protein ring not bound to DNA, because the *Z*-scale of the ScDmc1 ring is 0.7 ± 0.1 nm (see above). The second peak (~1.22 nm) likely represents the height of ScDmc1−ssDNA nucleoprotein complexes.

To determine whether ScDmc1 proteins bind ssDNA as protein rings or as helical filaments, we compared the FWHPs of ssDNA, RecA−ssDNA filaments, and ScDmc1−ssDNA filaments (Figure 3A−C). Histogram analysis indicates that the average FWHPs of ssDNA and RecA−ssDNA

helical filaments are 6.0 and 12.0 nm, respectively (Figure 3I). Intriguingly, the FWHP values of ScDmc1−ssDNA nucleoprotein complexes (Figure 2B) exhibit a bimodal distribution. The majority of ScDmc1−ssDNA nucleoprotein complexes (>80%) have an average FWHP of ∼17 nm, which is close to that of ScDmc1 protein rings (18.1 ± 2.6 nm; Figure 2C). A small fraction (∼10%) of ScDmc1−ssDNA nucleoprotein complexes have an average FWHP (∼13 nm) similar to that of RecA−ssDNA helical filaments (∼12 nm). Therefore, both rings and filamentous structures were found along single ssDNA molecules. Taken together, these results strongly suggest that the ScDmc1 protein is able to bind ssDNA as either a set of protein rings or a helical filament.

DISCUSSION

In this study, we first showed that the purified ScDmc1 protein exhibits much weaker recombinase activity than the *E. coli* RecA protein. AFM with CNT tips was used for direct visualization of both ScDmc1 protein rings and yDmc1−ssDNA nucleoprotein complexes. We found that most ScDmc1 proteins still associate with ssDNA as protein rings, and only a small fraction bind ssDNA to form filamentous structure. These results provide an explanation for the relatively low recombinaase activity of ScDmc1 as compared to RecA under the conditions examined if it is assumed that only the helical form is active in strand assimilation.

In this study, we successfully applied AFM with CNT tips to visualize ScDmc1 protein rings and ScDmc1−ssDNA nucleoprotein complexes. CNT tips possess many unique properties that make them ideal AFM probes. Nanotubes elastically buckle rather than break when deformed, which results in highly robust probes. Their high aspect ratio provides faithful imaging of deep trenches, while good resolution is retained due to their nanometer-scale diameter. The resolution power of AFM in this study has been validated by direct visualization of the helical pitch (9.5 nm) of RecA−ssDNA nucleoprotein filaments without any deconvolution or reconstruction procedures (Figure 3A). This method allows us to distinguish two forms of ScDmc1 bound to ssDNA in the presence of AMP-PNP: a linear array of stacked ScDmc1 protein rings and the filamentous structure. The latter, as described above, is very likely to be the active form, even though it represents a minority of the observed structures (∼10%). Finally, we have successfully used the imaging capabilities of AFM to show that ScDmc1 itself forms octameric protein rings. It had been shown previously that the molecular volume of the individual proteins determined by AFM matches their expected molecular weight (*34*, *35*). This volume determination method also had been applied in studying protein−protein and protein−DNA interactions (*35*).

The functional form of HsDmc1 was originally thought to comprise stacked protein rings on ssDNA (*24*−*27*). Very significantly, a recent EM study showed that the HsDmc1 protein can bind ssDNA to form helical nucleoprotein filaments (*28*). Also, this HsDmc1 protein is very active in promoting D-loop formation (*28*), indicating that Dmc1-mediated recombinase activity is initiated through the nucleation of Dmc1 onto ssDNA in forming helical filaments. Our results in this study provide further support for the notion that only helical filaments are active, because we found that the low catalytic activity of the yDmc1 protein correlates very well with its poor ability to form nucleoprotein filaments. This result fits well with the results of previous studies showing that the active forms of other recombinases, including *E. coli* RecA (*14*, *15*), eukaryotic Rad51 (*12*, *13*, *18*), and archaeal RadA (*20*−*23*), are helical filaments on ssDNA. Dmc1 likely uses a catalytic mechanism similar to that used by other members of this protein family.

Why are HsDmc1 and ScDmc1 less likely to form helical filaments with ssDNA? First, it was reported that the ATP-regenerating system, pH, and physiological ionic strength of the buffer were crucial for formation of HsDmc1 nucleoprotein filaments (*28*). Second, ssDNA-binding protein RPA also is helpful in improving the catalytic activity of the HsDmc1 protein in vitro (*28*). Third, Dmc1 might need accessory factors to function in vivo. It was reported that yeast meiosis-specific Mei5 and Sae3 proteins act together with ScDmc1 during meiotic DNA recombination (*37*, *38*). Mei5, Sae3, and Dmc1 form a ternary and evolutionarily conserved protein complex in vivo. These three proteins are mutually dependent for their chromosome association (*38*), raising the possibility that Mei5 and Sae3 may be required for nucleation of the Dmc1 protein onto ssDNA in the formation of helical filaments. Finally, HsRad54B, an orthologue of yeast Rad54/Tid1 (*28*), yeast Hop2−Mnd1 complex (*39*), and mouse Hop2 protein (*40*) also can stimulate Dmc1 in a specific manner. It would be interesting to further study whether these protein factors influence the structure of Dmc1 on DNA.

ACKNOWLEDGMENT

We thank Wen-Mei Kung for assistance in ScDmc1 protein purification, Chung Wang (Institute of Molecular Biology, Academia Sinica) for help with the ATPase assay, and Douglas Bishop (University of Chicago, Chicago, IL) for providing additional ScDmc1 protein to confirm our AFM results and for comments on the manuscript. We are grateful to Andrew H.-J. Wang for his generous support to this study.

REFERENCES

1. Bergerat, A., de Massy, B., Gadelle, D., Varoutas, P. C., Nicolas, A., and Forterre, P. (1997) An atypical topoisomerase II from Archaea with implications for meiotic recombination, *Nature 386*, 414−417.
2. Keeney, S., Giroux, C. N., and Kleckner, N. (1997) Meiosis-specific DNA double-strand breaks are catalyzed by Spo11, a member of a widely conserved protein family, *Cell 88*, 375−384.
3. Allers, T., and Lichten, M. (2001) Differential timing and control of noncrossover and crossover recombination during meiosis, *Cell 106*, 47−57
4. Hunter, N., and Kleckner, N. (2001) The single-end invasion: An asymmetric intermediate at the double-strand break to double-Holliday junction transition of meiotic recombination, *Cell 106*, 59−70.
5. Borner, G. V., Kleckner, N., and Hunter, N. (2004) Crossover/noncrossover differentiation, synaptonemal complex formation, and regulatory surveillance at the leptotene/zygotene transition of meiosis, *Cell 117*, 29−45.
6. Bishop, D. K. (1994) RecA homologs Dmc1 and Rad51 interact to form multiple nuclear complexes prior to meiotic chromosome synapsis, *Cell 79*, 1081−1092.
7. Rockmill, B., Sym, M., Scherthan, H., and Roeder, G. S. (1995) Roles for two RecA homologs in promoting meiotic chromosome synapsis, *Genes Dev. 9*, 2684−2695.

8. Shinohara, A., Ogawa, H., and Ogawa, T. (1992) Rad51 protein involved in repair and recombination in *S. cerevisiae* is a RecA-like protein, *Cell 69*, 457−470.
9. Sung, P. (1994) Catalysis of ATP-dependent homologous DNA pairing and strand exchange by yeast RAD51 protein, *Science 265*, 1241−1243.
10. Hong, E. L., Shinohara, A., and Bishop, D. K. (2001) *Saccharomyces cerevisiae* Dmc1 protein promotes renaturation of single-strand DNA (ssDNA) and assimilation of ssDNA into homologous super-coiled duplex DNA, *J. Biol. Chem. 276*, 41906−41912.
11. Gasior, S. L., Olivares, H., Ear, U., Hari, D. M., Weichselbaum, R., and Bishop, D. K. (2001) Assembly of RecA-like recombinases: Distinct roles for mediator proteins in mitosis and meiosis, *Proc. Natl. Acad. Sci. U.S.A. 98*, 8411−8418.
12. Sung, P., Trujillo, K. M., and Van Komen, S. (2000) Recombination factors of *Saccharomyces cerevisiae*, *Mutat. Res. 451*, 257−275.
13. Ogawa, T., Yu, X., Shinohara, A., and Egelman, E. H. (1993) Similarity of the yeast Rad51 filament to the bacterial RecA filament, *Science 259*, 1896−1899.
14. Heuser, J., and Griffith, J. (1989) Visualization of RecA protein and its complexes with DNA by quick-freeze/deep-etch electron microscopy, *J. Mol. Biol. 210*, 473−484.
15. Umemura, K., Komatsu, J., Uchihashi, T., Choi, N., Ikawa, S., Nishinaka, T., Shibata, T., Nakayama, Y., Katsura, S., Mizuno, A., Tokumoto, H., Ishikawa, M., and Kuroda, R. (2001) Atomic force microscopy of RecA-DNA complexes using a carbon nanotube tip, *Biochem. Biophys. Res. Commun. 281*, 390−395.
16. Yu, X., and Egelman, E. H. (1997) The RecA hexamer is a structural homologue of ring helicases, *Nat. Struct. Biol. 4*, 101−104.
17. Baumann, P., Benson, F. E., Hajibagheri, N., and West, S. C. (1997) Purification of human Rad51 protein by selective spermidine precipitation, *Mutat. Res. 384*, 65−72.
18. Conway, A. B., Lynch, T. W., Zhang, Y., Fortin, G. S., Fung, C. W., Symington, L. S., and Rice, P. A. (2004) Crystal structure of a Rad51 filament, *Nat. Struct. Mol. Biol. 11*, 791−796.
19. Story, R. M., Weber, I. T., and Steitz, T. A. (1992) The structure of the *E. coli* RecA protein monomer and polymer, *Nature 355*, 318−325.
20. Yang, S., Yu, X., Seitz, E. M., Kowalczykowski, S. C., and Egelman, E. H. (2001) Archaeal RadA protein binds DNA as both helical filaments and octameric rings, *J. Mol. Biol. 314*, 1077−1085.
21. McIlwraith, M. J., Hall, D. R., Stasiak, A. Z., Stasiak, A., Wigley, D. B., and West, S. C. (2001) RadA protein from *Archaeoglobus fulgidus* forms rings, nucleoprotein filaments and catalyses homologous recombination, *Nucleic Acids Res. 29*, 4509−4517.
22. Wu, Y., He, Y., Moya, I. A., Qian, X., and Luo, Y. (2004) Crystal structure of archaeal recombinase RadA: A snapshot of its extended conformation, *Mol. Cell 15*, 423−435.
23. Lee, M.-H., Leng, C.-H., Chang, Y.-C., Chou, C.-C., Chen, Y.-K., Hsu, F.-F., Chang, C.-S., Wang, A. H.-J., and Wang, T.-F. (2004) Self-polymerization of archaeal RadA protein into long and fine helical filaments, *Biochem. Biophys. Res. Commun. 323*, 845−851.
24. Masson, J. Y., Davies, A. A., Hajibagheri, N., Van Dyck, E., Benson, F. E., Stasiak, A. Z., Stasiak, A., and West, S. C. (1999) The meiosis-specific recombinase hDmc1 forms ring structures and interacts with hRad51, *EMBO J. 18*, 6552−6560.
25. Passy, S. I., Yu, X., Li, Z., Redding, C. M., Masson, J. Y., West, S. C., and Egelman, E. H. (1999) Human Dmc1 protein binds DNA as an octameric ring, *Proc. Natl. Acad. Sci. U.S.A. 96*, 10684−10688.
26. Gupta, R., Golub, E., Bi, B., and Radding, C. M. (2001) The synaptic activity of HsDmc1, a human recombination protein specific to meiosis, *Proc. Natl. Acad. Sci. U.S.A. 98*, 8433−8439.
27. Kinebuchi, T., Kagawa, W., Enomoto, R., Tanaka, K., Miyagawa, K., Shibata, T., Kurumizaka, H., and Yokoyama, S. (2004) Structural basis for octameric ring formation and DNA interaction of the human homologous-pairing protein Dmc1, *Mol. Cell 14*, 363−374.
28. Sehorn, M. G., Sigurdsson, S., Bussen, W., Unger, V. M., and Sung, P. (2004) Human meiotic recombinase Dmc1 promotes ATP-dependent homologous DNA strand exchange, *Nature 429*, 433−437.
29. Shih, Y. P., Kung, W. M., Chen, J. C., Yeh, C. H., Wang, A. H., and Wang, T. F. (2002) High-throughput screening of soluble recombinant, *Protein Sci. 11*, 1714−1719.
30. Leng, C. H., Brodsky, J. L., and Wang, C. (1998) Isolation and characterization of a DnaJ-like protein in rats: The C-terminal 10-kDa domain of hsc70 is not essential for stimulating the ATP-hydrolytic activity of hsc70 by a DnaJ-like protein, *Protein Sci. 7*, 1186−1194.
31. Wang, T. F., Kleckner, N., and Hunter, N. (1999) Functional specificity of MutL homologs in yeast: Evidence for three Mlh1-based heterocomplexes with distinct roles during meiosis in recombination and mismatch correction, *Proc. Natl. Acad. Sci. U.S.A. 96*, 13914−13919.
32. Kolodner, R. (1980) Genetic recombination of bacterial plasmid DNA: Electron microscopic analysis of in vitro intramolecular recombination, *Proc. Natl. Acad. Sci. U.S.A. 77*, 4847−4851.
33. Chang, Y. C., Wang, D. C., Chang, C. S., and Tsong, T. T. (2003) Easy method to adjust the angle of the carbon nanotube probe of an atomic force microscope, *Appl. Phys. Lett. 82*, 3541−3543.
34. Schneider, S. W., Larmer, J., Henderson, R. M., and Oberleithner, H. (1998) Molecular weight of individual proteins correlate with molecular volumes measured by atomic force microscopy, *Eur. J. Physiol. 435*, 362−367.
35. Ratcliff, G. C., and Erie, D. A. (2001) A novel single-molecule study to determine protein−protein association constants, *J. Am. Chem. Soc. 123*, 5632−5635.
36. Ratchiff, D., Hafner, J. H., Cheung, C. L., Woolley, A. T., and Lieber, C. M. (2001) Structural and functional imaging with carbon nanotube AFM probes, *Prog. Biophys. Mol. Biol. 77*, 73−110.
37. Hayase, A., Takagi, M., Miyazaki, T., Oshiumi, H., Shinohara, M., and Shinohara, A. (2004) A protein complex containing Mei5 and Sae3 promotes the assembly of the meiosis-specific RecA homolog Dmc1, *Cell 119*, 927−940.
38. Tsubouchi, H., and Roeder, G. S. (2004) The budding yeast Mei5 and Sae3 proteins act together with Dmc1 during meiotic DNA recombination, *Genetics 168*, 1219−1230.
39. Chen, Y. K., Leng, C.-H., Olivares, H., Lee, M.-H., Chang, Y.-C., Kung, W.-M., Ti, S.-C., Lo, Y.-H., Wang, A. H.-J., Chang, C.-S., Bishop, D. K., Hsueh, Y.-P., and Wang, T.-F. (2004) Heterodimeric complexes of Hop2 and Mnd1 function with Dmc1 to promote meiotic homolog juxtaposition and strand assimilation, *Proc. Natl. Acad. Sci. U.S.A. 101*, 10572−10577.
40. Enomoto, R., Kinebuchu, T., Sato, M., Yagi, H., Shibata, T., Kurumizaka, H., and Yokoyama, S. (2004) Positive role of the mammalian TBPIP/HOP2 protein in DMC1-mediated homologous pairing, *J. Biol. Chem. 279*, 35263−35272.

BI048897Q